

Article

Utilization of Palm Oil Fuel Ash (POFA) as an Admixture for the Synthesis of a Gold Mine Tailings-Based Geopolymer Composite

Einstine M. Opiso ¹, Carlito Baltazar Tabelin ^{2,*}, Christian V. Maestre ³, John Paul J. Aseniero ⁴, Takahiko Arima ⁵ and Mylah Villacorte-Tabelin ⁶

¹ Geo-Environmental Engineering Group, Civil Engineering Department, Central Mindanao University, Maramag 8710, Philippines

² Department of Materials and Resources Engineering Technology, Mindanao State University—Iligan Institute of Technology, Iligan City 9200, Philippines

³ Physics Department, College of Science, De La Salle University, Manila 0922, Philippines

⁴ Materials Science and Engineering Program, University of the Philippines, Quezon City 1101, Philippines

⁵ Division of Sustainable Resources Engineering, Faculty of Engineering, Hokkaido University, Sapporo 060-8628, Japan

⁶ Premier Research Institute of Science and Mathematics (PRISM), Mindanao State University—Iligan Institute of Technology, Iligan City 9200, Philippines

* Correspondence: carlito.tabelin@gmail.com

Abstract: The repurposing of gold (Au) mine tailings from artisanal and small-scale mining (ASGM) operations via alkali activation technology is a promising strategy for waste reduction in developing countries. Direct activation of mine tailings, however, is challenging because these materials contain relatively low aluminum (Al)-bearing minerals. In this study, palm oil fuel ash (POFA) was elucidated as a high Al-bearing waste derived-admixture for the synthesis of an ASGM tailings-based geopolymer composite. Semi-quantitative XRD analysis showed that the tailings contained quartz (SiO₂) (~58%), pyrite (FeS₂) (~20%) and calcite (CaCO₃) (~15%) with minor to trace amounts of aluminosilicates (~7%). Substantial amounts of environmentally regulated pollutants such as mercury (Hg) (40 mg/kg), lead (Pb) (8430 mg/kg) and arsenic (As) (300 mg/kg) were also found in the tailings. SEM-EDS, XRD and ATR-FTIR results showed the successful formation of a hybrid geopolymer-CASH matrix, which improved the unconfined compressive strength (UCS) of geopolymer composites from ~5 MPa to ~7 MPa. Furthermore, POFA did not significantly affect the thermal resistivity of geopolymer composites based on thermal analysis. Finally, the TCLP results showed that the Pb leaching concentrations from ASGM tailings exceeded environmental standards (~15,000 µg/L), which was suppressed after alkali activation to 300–500 µg/L. This means that POFA addition to ASGM tailings-based geopolymer composite improved not only its applicability as backfill, pavements and bricks but also its ability to immobilize toxic elements.

Keywords: mine tailings; mechanical properties; leaching test; palm oil fuel ash; thermal property



Citation: Opiso, E.M.; Tabelin, C.B.; Maestre, C.V.; Aseniero, J.P.J.; Arima, T.; Villacorte-Tabelin, M. Utilization of Palm Oil Fuel Ash (POFA) as an Admixture for the Synthesis of a Gold Mine Tailings-Based Geopolymer Composite. *Minerals* **2023**, *13*, 232. <https://doi.org/10.3390/min13020232>

Academic Editor: Alexander Mikhailovich Kalinkin

Received: 15 December 2022

Revised: 19 January 2023

Accepted: 31 January 2023

Published: 6 February 2023



Copyright: © 2023 by the authors. Licensee MDPI, Basel, Switzerland. This article is an open access article distributed under the terms and conditions of the Creative Commons Attribution (CC BY) license (<https://creativecommons.org/licenses/by/4.0/>).

1. Introduction

The proliferation of artisanal and small-scale gold mining (ASGM) operations in the Philippines have been generating voluminous amounts of mine tailings contaminated with mercury (Hg) and other toxic elements such as arsenic (As), lead (Pb), copper (Cu) and zinc (Zn) [1,2]. Exacerbating the problem is the subsequent reprocessing of this waste through carbon-in-pulp (CIP) to extract residual gold (Au) not recovered by the preceding gravity separation–amalgamation process, an approach producing final tailings contaminated with both Hg and cyanide (CN[−]) [3,4]. These tailings are currently stored in makeshift tailing dams or stockpiled without proper containment facilities or even disposed of directly to nearby streams and open fields [5]. These disposal practices could cause short- and long-term damage to human health and the environment if left unabated [6].

When mine tailings are exposed to the environment, they are notorious for generating strongly acidic and heavy metal-contaminated leachates called acid mine drainage (AMD). Wang et al. [7], for example, evaluated the migration and transformation of cadmium (Cd), Zn, Pb and As in a smelting site in China and reported that one of the main sources of contamination were areas used for sulfide-rich concentrate storage. Sulfide minerals such as pyrite (FeS_2) were also noted as the primary source of AMD in old tailing storage facilities in Japan [8]. Aside from mining activities, heavy metals could be released from tailings and other waste streams generated by electronic waste (E-waste) recycling when disposed of improperly [9]. Because of this, there is a need to find alternative ways to sustainably manage these wastes and minimize their potentially deleterious impacts on society and the environment.

One approach gaining a lot of attention recently is the circular economy, a concept integrating systems engineering, waste reprocessing, waste stabilization and waste repurposing to recirculate as many materials, wastes and by-products as possible back into circulation. Industrial wastes, including mine tailings [10], sludges [11], mine by-products such as clays [12] and mine waste rocks [13], have been repurposed as fillers for civil construction [14] and inert backfills [15,16] as well as reprocessed to extract base metals such as Cu [17], Au [18] and critical minerals [19]. The direct repurposing of mine tailings and industrial wastes as filler materials for construction is, however, problematic because of the possible release of heavy metals into the environment [20,21]. A promising workaround to this problem is to passivate sulfide minerals during repurposing using alkali activation or geopolymerization. This technique is receiving a lot of attention because of its (i) lower carbon footprint compared with conventional concrete-based technologies [22], (ii) large waste reductions achieved by material repurposing [23] and (iii) immobilization of toxic elements inherently found in mine tailings [24,25].

Geopolymerization is the process of transforming aluminosilicate-rich materials into a covalently bonded 3D network composed of silicon (Si), oxygen (O) and aluminum (Al) ($-\text{Si}-\text{O}-\text{Al}-\text{O}-$)_n [26]. This reaction occurs when an aluminosilicate-rich material is mixed with a highly-concentrated alkali hydroxide or silicate solution, forming a mechanically stable material composed of amorphous polymeric structures with interconnected Si—O—Al bonds [27,28]. Geopolymerization can be divided into four sub-reactions: (i) dissolution in alkaline solution, (ii) reorganization and diffusion of dissolved ions, (iii) formation of small, coagulated structures and (iv) polycondensation of soluble species to form hydrated products [29]. The main advantage of geopolymers is their potential to replace ordinary Portland cement (OPC) because they exhibit excellent physico-chemical and mechanical properties such as low density, minimal microporosity or nanoporosity, thermal stability, negligible shrinkage, high strength, high surface hardness, as well as fire and chemical resistance comparable to OPC [30].

Several studies have reported the potential use of tailings from phosphate [31], bauxite [32], copper [33], iron [34], tungsten [35], vanadium [36] and gold [3] mines as starting material for geopolymerization. In our previous work on the characterization of mine tailings collected from an ASGM operation in Mindanao, Philippines, for example, it was found that the solidification–repurposing approach through geopolymerization was feasible because of the Si and Al species and clay minerals found in tailings [3]. However, the products of the direct activation of ASGM tailings exhibited low mechanical properties and poor thermal stability compared with activated mine tailings incorporated with a co-binder [37]. This limits the use of ASGM tailings in geopolymerization for various construction sectors and other innovative applications.

Introducing other co-binding or additive materials containing significant Al and Si species such as metakaolin and coal fly ash has been found to improve the strength development of geopolymers [38]. Among the many industrial wastes, one potentially promising material is palm oil fuel ash (POFA), a by-product of the palm oil industry, because it contains significant aluminosilicate species and is locally available in the Philippines. This waste is generated during the combustion of palm oil husks and kernel shells in steam

boilers. The use of POFA as an additive has been shown to improve the mechanical properties and strength development of geopolymer concrete [39,40], mortar [41,42] and fiber-reinforced materials [43,44]. Khankhaje et al. [44], for example, reported a 14% higher compressive strength of concrete when 40% of POFA was added as a cement replacement. POFA-bearing concrete also exhibited lower water permeability and higher chloride and sulfate resistance than OPC concrete. Similarly, POFA has been utilized in lightweight structural green concrete capable of developing 96% of its maximum compressive strength in 7 days [40].

To date, there are still limited works that have investigated the use of POFA as raw material for geopolymerization. The majority of studies on POFA have focused on its use as an additive to OPC to produce higher-strength concrete. Therefore, this study was conducted to investigate the effects of POFA on the physico-chemical properties, morphology and mineralogy of ASGM tailings-based geopolymer composite. Specifically, the objectives of this work were to (i) characterize the ASGM tailings and POFA samples, (ii) determine the effects of POFA addition on the chemical and mechanical properties of synthesized geopolymer and (iii) evaluate the stability of environmentally regulated elements in ASGM tailings after geopolymerization. These objectives were achieved by using X-ray fluorescence spectroscopy (XRF), X-ray powder diffraction (XRD), attenuated total reflectance Fourier transform spectroscopy (ATR-FTIR), scanning electron microscopy coupled with energy-dispersive X-ray spectroscopy (SEM-EDS) and the toxicity characteristic leaching procedure (TCLP). Furthermore, the strength development and thermal properties of the synthesized geopolymer composite (with and without POFA) were analyzed and quantified using the unconfined compressive strength test and thermogravimetry/differential thermal analysis (TG/DTA).

2. Experimental Design

2.1. Collection and Preparation of Materials

The ASGM tailings used in this study were collected from a tailings impoundment of a small-scale carbon-in-pulp (CIP) plant in Mainit, Davao de Oro (formerly Compostela Valley), Philippines while POFA was obtained from a palm milling company in Quezon, Bukidnon, Philippines. The samples were oven-dried, lightly crushed using an agate mortar and pestle and sieved through a 75 μm aperture screen. The POFA sample contained quartz, muscovite, dolomite and mullite, and was composed of 46% SiO_2 , 5.5% Fe_2O_3 , 10.4% Al_2O_3 , 0.7% SO_3 , 7.4% CaO and 7.3% Na_2O [5]. For the powder activator, sugar mill lime sludge was obtained from a sugar milling company in Butong, Quezon, Bukidnon, Philippines. Collection and preservation of ASGM tailings samples were completed following ASTM-D4220 (standard practices for preserving and transporting soil samples). The lime sludge sample was directly screened after drying and crushing to obtain a particle size distribution of $>200 \mu\text{m}$.

2.2. Synthesis of Powder Activator and Geopolymer Composite

The preparation of sugar mill lime sludge-based powder activator (PA) was completed by replicating the procedure proposed by Aseniero et al. [3]. The sludge was first mixed with 5M NaOH solution at a mixing ratio of 0.5 by weight for 10 min in a rotary mixer. The resulting paste was then dried in an oven for 8 h at a temperature of 80°C, cooled, pulverized and sieved to attain a particle size of $<150 \mu\text{m}$. The resulting PA was composed of 5% SiO_2 , 0.2% Fe_2O_3 , 1.4% Al_2O_3 , 3.5% SO_3 , 44% CaO and 12% Na_2O while mineralogically, it contained quartz, calcite, portlandite, sodium nitrate and lime [5].

The synthesis of geopolymer composites was completed by mixing the powder activator, ASGM tailings, POFA and 20% water equivalent to the total weight of the solid sample using the mixing design summarized in Table 1. These formulations were based on the optimum mixing ratio with the best mechanical properties obtained in our previous published work [4]. The mixture was stirred at median speed in a rotary mixer for at least 10 min to ensure the sufficient dissolution of silicates and aluminates under alkaline

conditions. The pastes were then poured into non-reactive 50 × 50 × 50 mm cubic molds and shaken using a vibrating table for 2 min to remove air pockets. The samples were then covered to avoid loss of water and allowed to set under ambient conditions. After 5 days, the geopolymer composites were de-molded and cured for 14 days. The synthesized geopolymer composites were labeled as GPA (without POFA) and GPF (with POFA).

Table 1. Geopolymer composite mixing design.

Sample	ASGM Tailings (%)	POFA (%)	PA (%)
GPA	50	0	50
GPF	50	10	40

2.3. Characterization of Gold Mine Tailings and Geopolymer Composite

Preliminary analysis of ASGM tailings was conducted to determine its suitability as source material for geopolymerization. Particle size distribution of the subsamples was determined in deionized water using laser diffraction (Microtrac[®] MT3300SX, Nikkiso Co., Ltd., Tokyo, Japan) with a measuring capability between 0.02 and 2800 µm. For the chemical composition and ATR-FTIR analysis of raw materials and synthesized geopolymer composites, the samples were manually ground using an agate mortar and pestle to <50 µm and then analyzed by XRF (loose powder method; NEXCG, Rigaku Corporation, Tokyo, Japan) and FT/IR-6200 HFV with ATR ProOne[®] attachment equipped with a diamond prism (Jasco Analytical Instruments, Tokyo, Japan). The mineralogical compositions of the samples were identified using XRD (MultiFlex, Rigaku Corporation, Tokyo, Japan) on <50 µm pressed powders and the patterns were analyzed by Match![®] software (Crystal Impact, Bonn, Germany).

To identify the morphological properties and to conduct additional elemental analysis of the samples, an SEM-EDS (InTouchScope[™], JSM-IT200, JEOL Ltd., Tokyo, Japan) was used. Meanwhile, the thermal properties of synthesized products were determined by Thermogravimetry/Differential Thermal Analysis (TG/DTA) using Perkin Elmer STA 6000 with a heating range from 30 to 950 °C. This procedure was carried out by heating the samples in a nitrogen atmosphere at 50 mL/min up to 900 °C using the simultaneous thermal analyzer. Finally, the synthesized geopolymer composites were subjected to the universal compressive strength (UCS) test following ASTM D5102-96 (Standard Test Method for Unconfined Compressive Strength of Compacted Soil-Lime Mixtures). Before the UCS test, the geopolymer composites were polished and cleaned to make sure that they had a smooth and flat surface to avoid discrepancies in the test results.

2.4. Toxicity Characteristic Leaching Procedure

The toxicity characteristic leaching procedure (TCLP) was employed following USEPA 1311 to determine the leachabilities of environmentally regulated contaminants such as cyanide (CN⁻), As, Hg, Pb and selenium (Se) found in ASGM tailings and geopolymer composites. Selected samples were subjected to a 0.57% acetic acid (CH₃COOH) solution at a liquid-to-solid ratio of 20 and shaken for 12 h at 50 rpm under ambient conditions. The leachates were collected by vacuum filtration using 0.45 µm MCE membrane filters and stored in an amber bottle. The concentrations of the selected contaminants in the leachates were determined by inductively coupled plasma optical emission spectroscopy (ICP-OES, Agilent 5100, Argilent Technologies, Inc., Santa Clara, California, USA) (margin of error = ±2%) while CN⁻ was measured using atomic absorption spectroscopy (AAS). Figure 1 illustrates the actual experimental setup of TCLP.

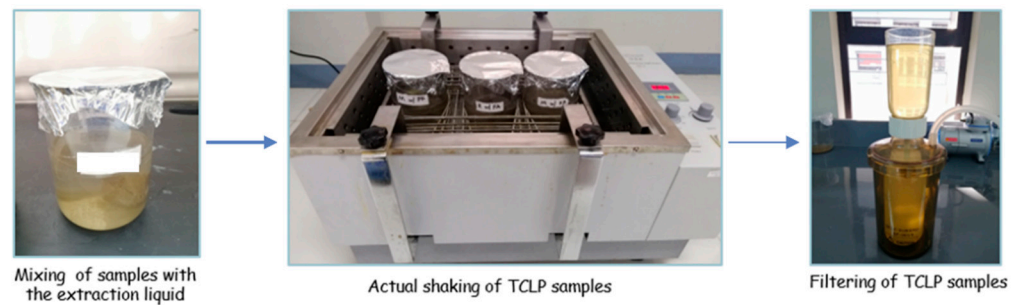


Figure 1. A schematic diagram of the TCLP setup.

3. Results

3.1. Physico-Chemical, Mineralogical and Morphological Properties of Tailings

The particle size distribution of ASGM tailings is shown in Figure 2a. A gap-graded distribution was observed and the sample had a D_{80} of 18.94 μm . Based on the unified soil classification system (USCS), the sample consisted predominantly of clay-sized particles with traces of silty sand-sized materials. The ASGM tailings were mainly composed of Si (48.1% as SiO_2) with moderate amounts of Al (8.9% as Al_2O_3) (Figure 2c). The Fe (6.38%) and S (0.28%) of the ASGM tailings were substantial, indicating that sulfide minerals such as pyrite and chalcopyrite were present in the sample. This deduction was also supported by the photomicrographs of ASGM tailings as shown in Figure 2b. Moreover, XRF analysis detected Hg, Pb and As in the sample at 40 mg/kg, 8430 mg/kg, and 300 mg/kg, respectively.

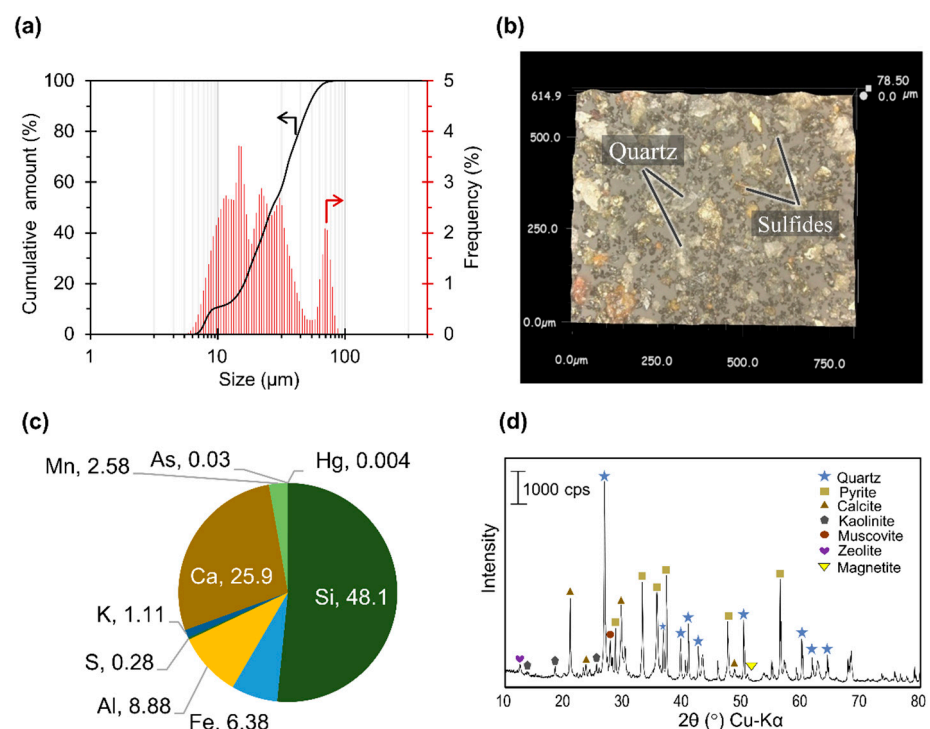


Figure 2. (a) Particle size distribution, (b) photomicrograph, (c) chemical composition and (d) XRD pattern of the ASGM tailings sample used in this study.

Mineralogically, the ASGM tailings composed mainly of quartz (SiO_2) (JCPDS card No. 96-900-5021), pyrite (FeS_2) (JCPDS card No 96-901-5843), and calcite (CaCO_3) (JCPDS card No 96-901-4745) with minor amounts of magnetite (Fe_3O_4) (JCPDS No 19-0629), kaolinite ($\text{Al}_2\text{Si}_2\text{O}_5(\text{OH})_4$) (JCPDS card No 96-155-0599), zeolite ($\text{Na}_2\text{Al}_2\text{Si}_2\text{O}_8$) (JCPDS card No 96-810-1550) and muscovite ($\text{KAl}_2(\text{FOH})_2$, or $(\text{KF})_2(\text{Al}_2\text{O}_3)_3(\text{SiO}_2)_6$) (JCPDS card No 96-

110-1033) (Figure 2d). Semi-quantitative analysis of the sample using Match![®] revealed that quartz was the dominant mineral at about 58%. Moreover, the broad peak between 25° and 26° observed in the samples could be attributed to the presence of amorphous to poorly crystalline phases of aluminosilicates, which are highly reactive and soluble in basic solution. The ASGM tailings sample, however, had low abundances of clay and phyllosilicate minerals (2.8% of kaolinite, 1.8% of zeolite and 1.9% of muscovite). Finally, substantial amounts of pyrite (about 20%) were found in the ASGM tailings sample.

Morphological characteristics and elemental compositions of particles present in ASGM tailings were determined by SEM-EDS. The sample had angular/irregular particles with fine-sized particles agglomerated or attached to coarse particles. SEM-EDS point analysis showed that particles in the ASGM tailings were mainly composed of Si, Ca, Al, Fe, S and O, which corroborated the XRF results. An Fe- and S-rich particle was also observed by SEM-EDS (Figure 3e).

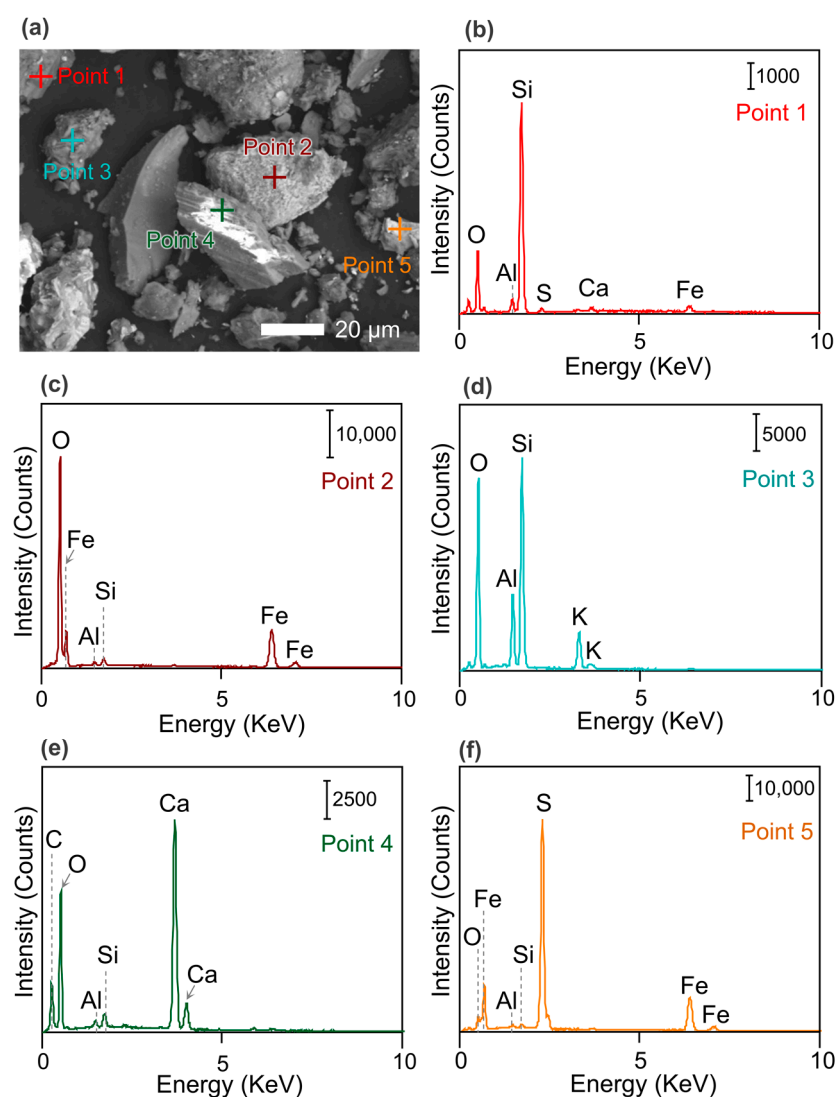


Figure 3. Photomicrograph of ASGM tailings (a) and the corresponding elemental point analysis of selected particles: Point 1 (b), Point 2 (c), Point 3 (d), Point 4 (e) and Point 5 (f). Note the differences in the scale of the y-axis of the EDS spectra.

Infrared vibrational bands attributed to Al and Si were detected by ATR-FTIR as illustrated in Figure 4. An absorption broad peak of Al in octahedral coordination with hydroxyl (OH) groups (Al—OH) was observed at 3620 cm^{-1} , which indicates that amorphous to poorly crystalline phyllosilicate phases were present in the samples [45]. Moreover,

the mid-infrared to low-infrared spectral range ($1200\text{--}400\text{ cm}^{-1}$) showed characteristic IR bands of aluminosilicate minerals. Among these characteristic bands was the broad peak detected at $1160\text{--}955\text{ cm}^{-1}$, which was attributed to the asymmetric stretching vibration of Si—O—Al or Al—O—Si [5,46]. Meanwhile, the peaks at 776 cm^{-1} and 695 cm^{-1} were assigned to the tetrahedral–tetrahedral ion vibration of silicates such as quartz [46]. Furthermore, the absorption band observed at 874 cm^{-1} corresponded to Al octahedral crystals [46]. Meanwhile, the IR peak at 462 cm^{-1} was attributed to Si—O—Si stretching vibration [5] and that at 2510 cm^{-1} corresponded to Al—O—H stretching and/or Si—O—Si stretching [45,46]. The broad spectrum from $3000\text{ to }3800\text{ cm}^{-1}$ corresponded to adsorbed H—O—H [47,48] while the intense vibrational peak at 1421 cm^{-1} was due to the C—O stretching vibration of CaCO_3 [46,49]. Deconvoluted regions of the FTIR spectrum revealed additional absorption bands at 1555 , 1478 , 1453 and 1421 cm^{-1} , which were assigned to carbonate-type complexes formed on pyrite [50]. The presence of this type of band was probably influenced by the constant exposure of this pyrite in the tailings to the air causing its reaction with atmospheric CO_2 . Meanwhile, the IR peaks at 532 cm^{-1} and 462 cm^{-1} were assigned to Fe—O stretching bands of Fe—O—Si [50] and iron oxides [51], respectively.

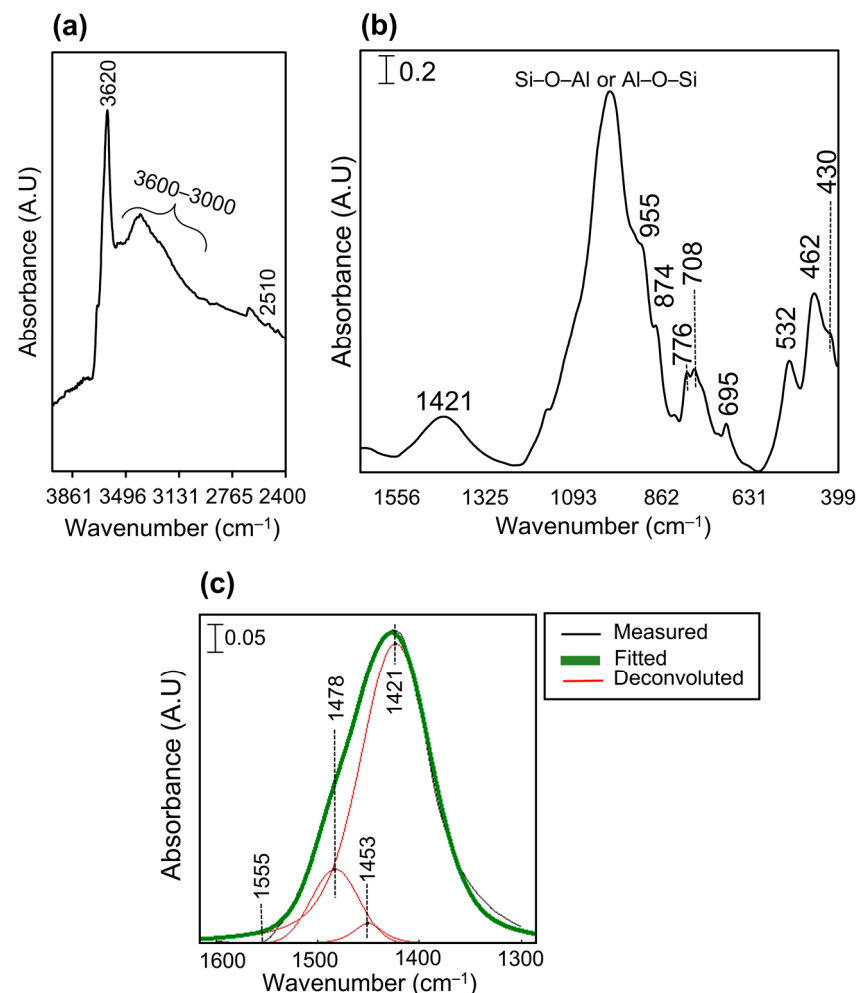


Figure 4. FTIR spectrum of the ASGM tailings sample: (a) $4000\text{--}2400\text{ cm}^{-1}$, (b) $1600\text{--}399\text{ cm}^{-1}$, and (c) deconvoluted spectrum between 1650 and 1250 cm^{-1} .

3.2. Effects of Palm Oil Fuel Ash on the Properties of Geopolymer Composites

As shown in Figure 5, the synthesized geopolymer composites had similar mineralogical properties. The detected minerals included quartz (SiO_2) (JCPDS card No. 96-900-5021), pyrite (FeS_2) (JCPDS card No 96-901-5843), calcite (CaCO_3) (JCPDS card No 96-901-4745),

kaolinite ($\text{Al}_2\text{Si}_2\text{O}_5(\text{OH})_4$) (JCPDS card No 96-155-0599), muscovite ($\text{KAl}_2(\text{FOH})_2$) (JCPDS card No 96-110-1033), zeolite ($\text{Na}_2\text{Al}_2\text{Si}_2\text{O}_8$) (JCPDS card No 96-810-1550), magnetite (Fe_3O_4) (JCPDS No 19-0629) and calcium aluminum silicate hydrate (CASH) (ICDD 00-055-0738). Semi-quantitative analysis of the XRD patterns showed that calcite (CaCO_3) (GPF = 43%; GPA = 49%) and quartz (GPF = 18%; and GPA = 20%) predominated in the synthesized materials. It was also observed that phyllosilicates and clay minerals were more prevalent in GPF, which could be attributed to the addition of these minerals from POFA.

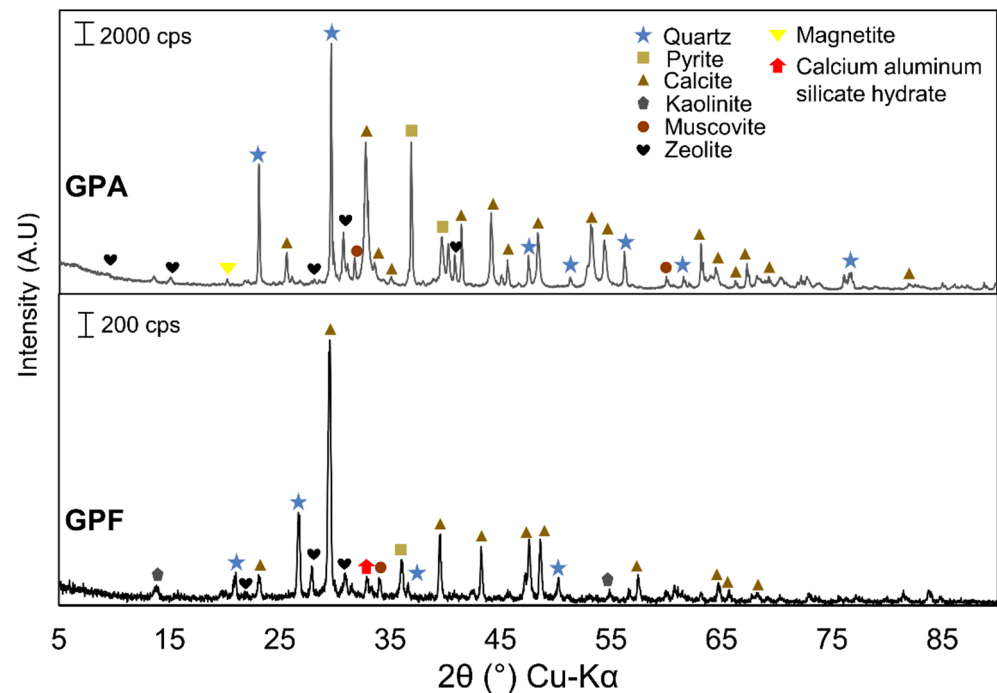


Figure 5. XRD patterns of synthesized geopolymers without POFA (GPA) and with POFA (GPF).

The FTIR spectra of synthesized geopolymers are illustrated in Figure 6. An IR absorption broad band of Al in octahedral coordination with OH groups was observed at 3620 cm^{-1} in both geopolymers, which was also noted in the IR spectrum of ASGM tailings (Figure 4). The mid-infrared to low-infrared spectral regions ($1200\text{--}400\text{ cm}^{-1}$) of the synthesized geopolymers were also very similar to that observed in ASGM tailings. However, some of the adsorption bands shifted and their intensities changed after alkali activation. The broad asymmetric stretching vibration of Si—O—Al or Al—O—Si centered at 1005 cm^{-1} and shifted to 1010 cm^{-1} in both geopolymers while that at 693 cm^{-1} moved to 712 cm^{-1} and 710 cm^{-1} for GPA and GPF, respectively. Additionally, the peak attributed to the tetrahedral–tetrahedral ion vibration of silicate shifted from 776 cm^{-1} to 796 cm^{-1} . Similar shifting of the Si—O—Si stretching vibration from 456 cm^{-1} to 459 cm^{-1} was observed in the geopolymers. Meanwhile, some absorption bands were retained after geopolymerization such as the Si—OH bending mode or the tetrahedral bending of Al at 874 cm^{-1} and peaks associated with Fe—O stretching at 532 cm^{-1} .

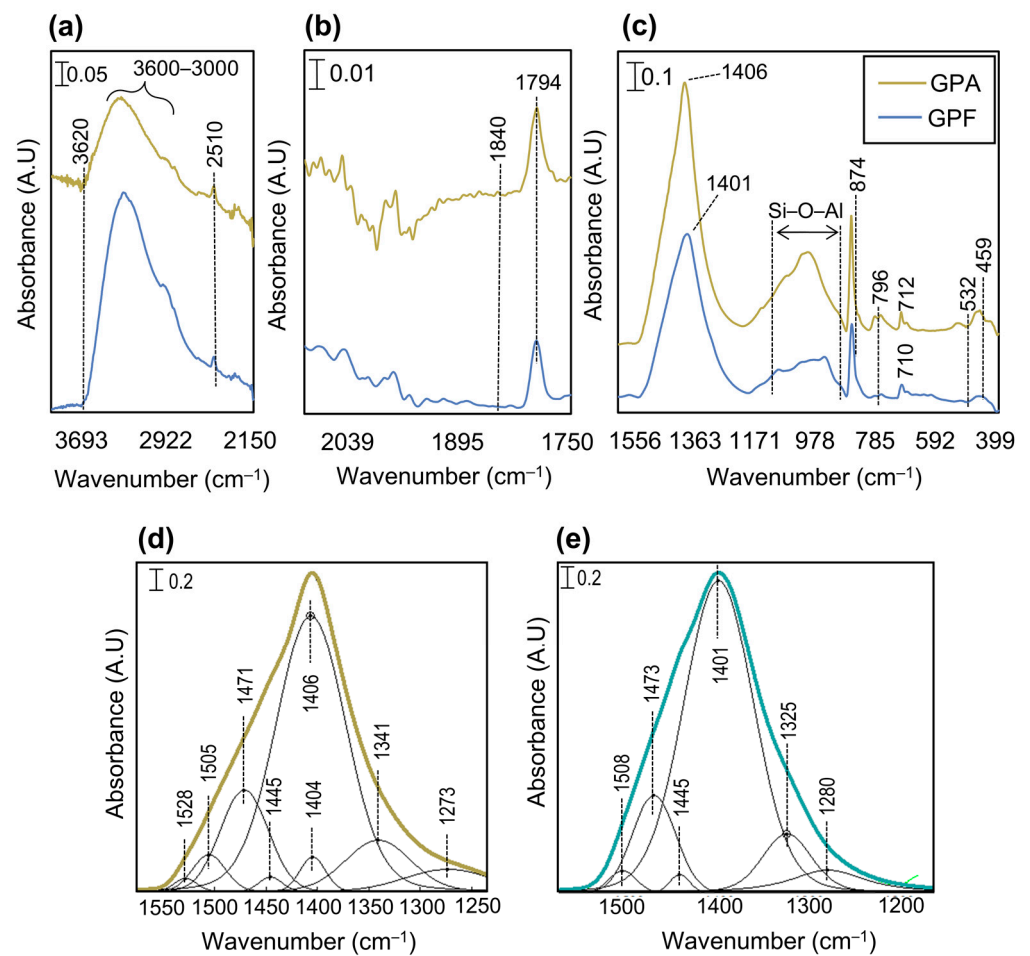


Figure 6. FTIR spectra of synthesized geopolymer composites: (a) 4000–2150 cm^{-1} , (b) 2140–1750 cm^{-1} , (c) 1600–400 cm^{-1} and deconvoluted spectra between 1600 and 1200 cm^{-1} for GPA (d) and GPF (e). Note that the black plots in (d,e) are deconvoluted peaks.

The absorption broad peak around 3350 cm^{-1} and 1840 cm^{-1} was due to the OH stretching vibrations of adsorbed and crystalline water, respectively (Figure 6). The strongest IR absorbance peaks for synthesized geopolymer composites were observed at 1401 cm^{-1} for GPF and 1406 cm^{-1} for GPA, which corresponded to the vibrations of C—O coordinated with Ca. Deconvolution of the regions between 1600 and 1200 cm^{-1} of the geopolymer composites showed additional peaks assigned to carbonate-type complexes formed on pyrite.

Representative samples of the geopolymer composites were examined for their microstructural characteristics using SEM-EDX. The morphologies of geopolymer composites are shown in Figure 7 for GPA and Figure 8 for GPF as well as the corresponding elemental maps of Mg, O, Na, Fe, S, Ca, Al and Si. Coarse surface topology was observed in all synthesized geopolymer samples. Some asymmetrically shaped particles of ASGM tailings (Figure 3) were dissolved after geopolymerization and a “gel-like” structure was formed in both samples, which could be attributed to amorphous and poorly crystalline phases formed by geopolymerization as noted in the FTIR results. Meanwhile, Ca dominated the entire mapped area and was detected in the same areas as Si and Al. Meanwhile, Al, Si, K, Mg and oxygen (O) were observed in the same region. It is also important to note that Fe and S appeared on the sample region of the GPF samples.

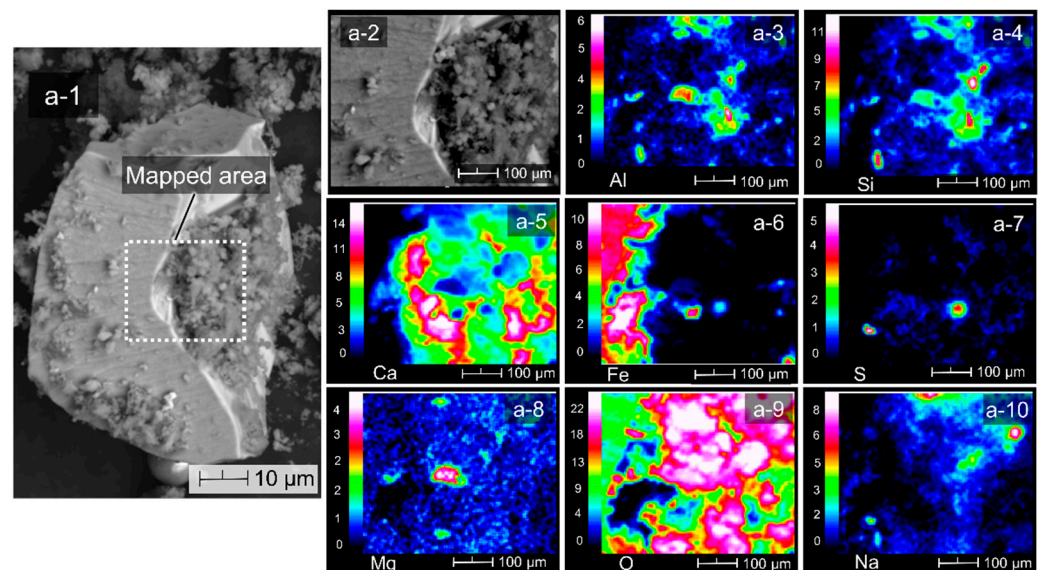


Figure 7. (a-1) Photomicrograph of GPA and (a-2) the mapped area with corresponding elemental maps of Al (a-3), Si (a-4), Ca (a-5), Fe (a-6), S (a-7), Mg (a-8), O (a-9) and Na (a-10).

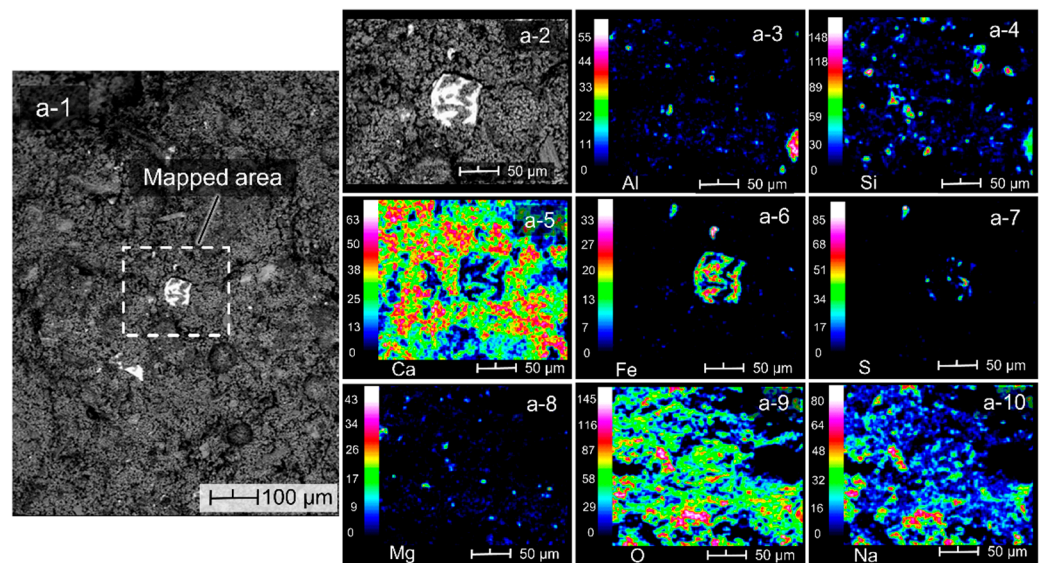


Figure 8. (a-1) Photomicrograph of GPF and (a-2) mapped area with corresponding elemental maps of Al (a-3), Si (a-4), Ca (a-5), Fe (a-6), S (a-7), Mg (a-8), O (a-9) and Na (a-10).

3.3. Effects of Palm Oil Fuel Ash on the Mechanical, Thermal and Leaching Properties of Geopolymer Composites

The mechanical property of synthesized geopolymer composites after 14 days of curing was determined using the UCS test as shown in Figure 9. Both composites had remarkable mechanical strength with average UCS values of 7.58 MPa for GPF and 5.48 MPa for GPA. It was observed that the addition of 10% POFA increased the strength of geopolymer composites by approximately 28%.

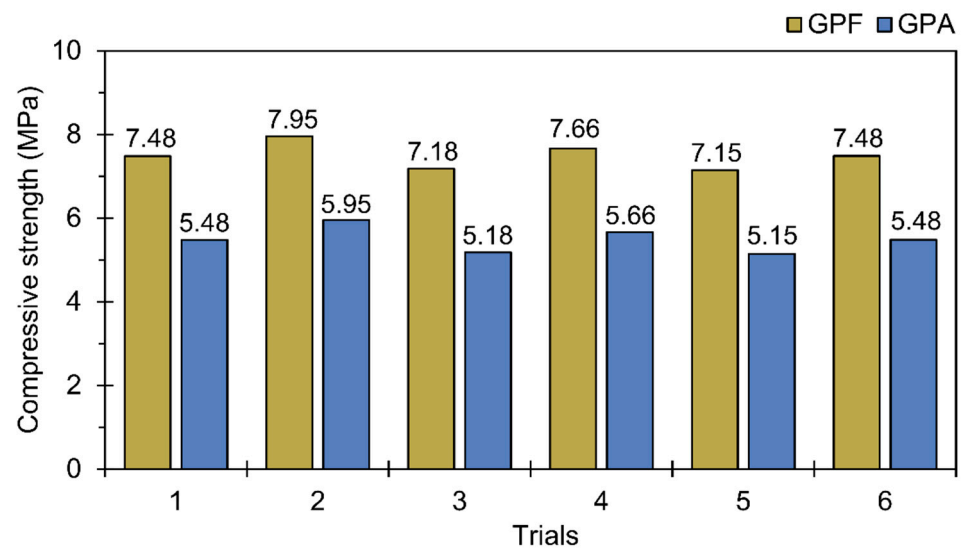


Figure 9. Unconfined compressive strengths (UCS) of geopolymer composites without POFA (GPA) and with POFA (GPF).

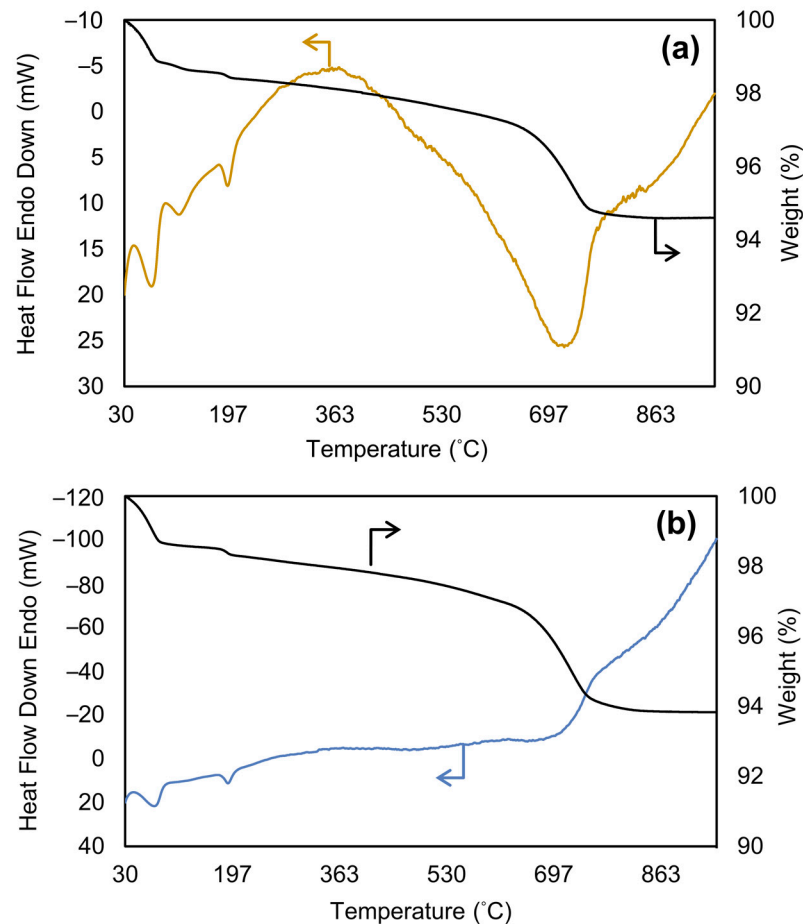
The TG-DTA curves of geopolymer composites are shown in Figure 10. Evident weight losses, corresponding peak temperatures and effective temperature ranges are also presented in Table 2 while Table 3 lists the DTA peak temperatures. In general, no significant differences were observed concerning the thermal resistivity of both samples. One endothermic peak for both samples at 30–135 °C appeared on the DTA graph, which could be attributed to the dehydration of absorbed water [52] with a mass loss of around 2–8%. Meanwhile, another endothermic peak located around 175 °C was observed in GPF with a weight loss of approximately 9%. Furthermore, continuous degradation and an endothermic peak were found between 200 and 600 °C corresponding to the dehydroxylation of the OH groups [53]. Finally, the intensive endothermic peak from 600 to 800 °C was due to the de-carbonation of CaCO₃, which had the highest mass loss at approximately 16% and 15% for GPF and GPA, respectively.

Table 2. TG-DTA data of the geopolymer composites.

Sample ID	Weight Loss, % with the Corresponding Peak Temperature	Peak Temperature (Tp), °C	Temperature Range, °C
GPF	Weight loss 1 = 7.345	Tp1 = 58.94 Tp2 = 175.51 Tp3 = 720.65	30.00–134.88 134.88–197.70 606.89–899.16
	Weight loss 2 = 1.384		
	Weight loss 3 = 6.850		
	Weight loss 4 = 16.837		
	Weight loss 5 = 0.026		
	Residue = 67.558		
GPA	Weight loss 1 = 5.846	Tp1 = 56.85 Tp2 = 105.62 Tp3 = 177.61 Tp4 = 395.21 Tp5 = 423.22 Tp6 = 723.70	30.00–81.30 81.30–139.95 139.95–209.64 384.40–409.89 409.89–435.05 534.46–807.77
	Weight loss 2 = 1.205		
	Weight loss 3 = 1.146		
	Weight loss 4 = 1.807		
	Weight loss 5 = 0.393		
	Weight loss 4 = 0.420		
	Weight loss 5 = 1.728		
Weight loss 6 = 15.855			
	Weight loss 7 = 0.059		
	Residue = 71.541		

Table 3. DTA peak temperature of the geopolymer composites.

Sample ID	Peak Temperature (T_p), °C
GPF	Tp1 = 63.70 (endothermic) Tp2 = 178.43 (endothermic) Tp3 = 701.19 (endothermic)
GPA	Tp1 = 107.80 (endothermic) Tp2 = 180.33 (endothermic) Tp3 = 710.00 (endothermic)

**Figure 10.** TG-DTA curve with DTA for (a) GPA (without POFA) and (b) GPF (with POFA).

The leachabilities of environmentally regulated elements in ASGM tailings and geopolymer composites are summarized in Table 4. Among the five contaminants found in the sample, the leachability of Pb was more than 15,000 µg/L, which exceeded the standard by more than 3-fold. In comparison, the leachabilities of As, Hg and Se were below the environmental standards at 149 µg/L, 76.5 µg/L and 17.5 µg/L, respectively. Meanwhile, cyanide (CN⁻) was detected in the leachate of ASGM tailings at 1.2 µg/L, despite the instability and high degradation of this compound when exposed to air, water and sunlight. In the environment, CN⁻ is mostly associated with Fe, forming complexes such as Fe(CN)₆³⁻ and Fe(CN)₆⁴⁻, which have a lower toxicity but could be converted back to free cyanide under certain conditions [54]. Furthermore, the leachability results of the geopolymer composites showed that GPF had the lowest leaching concentrations of the five contaminants. For example, the leaching concentration of Pb was reduced from 15,360 µg/L to 379 µg/L.

Table 4. TCLP leachability characteristics of ASGM tailings and synthesized geopolymers composites ($\mu\text{g/L}$).

Samples	As	Hg	Pb	Se	CN ⁻
Standards (DENR)	5000	200	5000	1000	–
Standards (EPA)	2800	5000	5000	1000	–
ASGM tailings	149	76.5	15,360	17.5	1.2
GPA	41.6	0.9	509	6.3	<0.1
GPF	24.0	<0.1	379	2.7	<0.1

Note: “–” means not detected.

4. Discussion

The ASGM tailings collected from Mainit, Davao de Oro were mainly composed of quartz, with moderate amounts of calcite and pyrite as well as minor to trace amounts of kaolinite, zeolite, muscovite and magnetite. The identification of these minerals by XRD was consistent with the XRF, SEM-EDS and ATR-FTIR results. In addition, a broad XRD peak between 25° and 26° (Figure 2) together with the OH group infrared absorption band observed at 3620 cm^{-1} (Al—OH) (Figure 4) implied that amorphous to poorly crystalline phyllosilicate phases were present in the sample [46]. Among the minerals and phases identified above, only amorphous phases [4], zeolite [55], kaolinite [56] and muscovite [57] will participate during alkali activation because they readily dissolve under alkaline conditions. The rest of the minerals such as quartz and calcite are stable under alkaline conditions, so they would act as filler materials and become “aggregates” in geopolymers composites. The substantial amounts of calcite (~26% Ca) measured in the ASGM tailings could be attributed to the (i) use of lime—a well-known compound that transforms to calcite in the environment—for pH control during the CIP process, and (ii) the innate characteristics of the gold ore [58]. The presence of Ca-bearing minerals is an advantage for repurposing the tailings into construction materials because they are essential in the formation of pozzolanic minerals, which could enhance the strength and thermal stability of synthesized geopolymers composites. These results suggest that the ASGM tailings sample from Mainit, Davao de Oro is suitable as a raw material for geopolymers polymerization.

The XRF results detected substantial amounts of Hg (40 mg/kg), Pb (8430 mg/kg) and As (300 mg/kg) in the ASGM tailings sample at concentrations higher than the average content found in soils and sediments. On average, soils and rocks contain Pb and As at around 7–150 mg/kg and 1–10 mg/kg, respectively [2]. Mercury was most likely introduced due to elemental Hg added during amalgamation while As and Pb are found in the tailings as impurities in sulfide minerals such as pyrite [4,59].

Mercury and Pb are toxic heavy metals notorious for causing Minamata disease and damage to the central nervous system, respectively. Meanwhile, As is a metalloid reported to increase the risks of developing skin, lung, kidney and liver cancers even in minute concentrations upon prolonged exposure [1,7]. Based on the standards set by the United States Environmental Protection Agency (USEPA) and the hazardous waste management section of the Department of Environmental and Natural Resources (DENR) of the Philippines, the ASGM tailings from Mainit, Davao de Oro can be classified as hazardous wastes because of the high leachability of lead (Pb). Although the leachabilities of As and Hg were both below the environmental standards, the release of these toxic elements should be limited as much as possible because they are notorious for bioaccumulating in food crops such as rice as well as causing serious and adverse health effects when constantly ingested at trace amounts (i.e., chronic poisoning) [8].

The addition of POFA during the alkali activation of ASGM tailings improved the UCS of geopolymers composites by ~28%. The higher mechanical properties of the synthesized

product could be attributed to the (1) addition of amorphous or poorly crystalline silica and aluminosilicates, (2) the formation of CASH and (3) the reduction in microstructure porosity. Poorly crystalline silica, aluminosilicate and calcium species found in POFA readily dissolved during geopolymerization and generated the 3D $(\text{—Si—O—Al—O—})_n$ network. The formation of this geopolymer matrix was supported by the shifting of IR bands of Si—O—Al or Al—O—Si and Si—O—Si (Figures 4 and 6). According to He et al. [60], alkali activation not only generated a 3D geopolymer matrix but also reduced the porosity via dissolution–transformation–reformation that translated to a higher mechanical strength. Similarly, the addition of CaO from POFA was an important factor explaining the strength of geopolymer composites because it induced the formation of CASH. The enhanced formation of CASH after the addition of POFA was confirmed by the more pronounced CASH XRD peak (Figure 5) and the higher thermogravimetric weight loss measured at 175 °C (Figure 10), which is related to the dehydration of CASH [29]. Finally, the high abundance of CaCO_3 in POFA improved the mechanical properties of synthesized products via the porosity reduction in the microstructure. Although porosity was not measured in this work, previous studies have shown that CaCO_3 lowered pore spaces during alkali activation [28], resulting in higher compressive strengths [61]. It is noteworthy that the 7.1–8 MPa UCS obtained in this work is comparable to the conventional strength of concrete and supported the successful synthesis of ASGM tailings-based geopolymer composites. Moreover, as stated by the standard set by the National Structural Code of the Philippines, compressive strength at these values can be recommended for backfill application.

Alkali activation limited the leachabilities of As, Hg, Pb, Se and CN^- from ASGM tailings with the lowest leaching concentrations observed after the addition of POFA. For example, the TCLP leaching concentration of Pb was reduced from 15,360 $\mu\text{g/L}$ to 379 $\mu\text{g/L}$ after geopolymerization with POFA. It was also observed that the leachabilities of As, Hg and Se had significant reductions in GPF while that of CN^- was below the instrumental detection limit. This substantially lower contaminant leaching from the tailings could be attributed to the passivation of pyrite and elemental Hg via physical–chemical encapsulation. This deduction is supported by the SEM-EDS results showing the geopolymer matrix covering pyrite particles (Figures 7 and 8) and the IR signatures of carbonate groups reacting with FeOOH on the surface of the pyrite (Figure 6), a reaction well-known in mine tailings, pyrite-rich construction wastes and aquifer sediments [62,63]. Moreover, carbonate minerals in POFA could neutralize AMD [8], promote the precipitation of Pb [21] and sequester dissolved As via adsorption [2]. Based on these results, the addition of POFA not only improved the mechanical properties of ASGM tailings-based geopolymer composites but also enhanced their environmental stability via mineral encapsulation and immobilization reactions (e.g., adsorption and precipitation).

5. Conclusions

This study investigated the utilization of POFA as an admixture for the synthesis of ASGM tailings-based geopolymer composites and identified its physico-chemical, mineralogical and morphological properties. Mechanical and thermal properties, including the geochemical stability of toxic heavy metals and metalloids, were also evaluated. The major findings of this study are summarized as follows:

1. ASGM tailings from Mainit, Davao de Oro are mainly composed of quartz, pyrite and calcite with trace to minor amounts of aluminosilicate minerals;
2. Insignificant transformations were observed in the IR spectroscopic and mineralogical characteristics of geopolymer composites after the addition of POFA;
3. Morphological and elemental analysis revealed the encapsulation/immobilization of sulfide minerals due to alkali activation;
4. Introduction of POFA as an admixture enhanced the mechanical properties of the ASGM tailings-based geopolymer composites by about 28%;
5. Insignificant differences were observed in the thermal resistivity of the geopolymer composites after the addition of 10% POFA;

6. The addition of POFA during alkali activation enhanced the immobilization of Hg, Pb, As, Se and CN^- from the ASGM tailings via encapsulation and adsorption/precipitation.

Author Contributions: Conceptualization and methodology, E.M.O., C.V.M. and J.P.J.A.; investigation, E.M.O., C.B.T., C.V.M., J.P.J.A., T.A., and M.V.-T.; data curation, E.M.O., C.B.T., C.V.M., J.P.J.A., T.A., and M.V.-T.; writing—original draft preparation, E.M.O., C.B.T. and C.V.M.; writing—review and editing, E.M.O., C.B.T., C.V.M., T.A., and M.V.-T.; literature research, E.M.O., C.B.T., C.V.M. and J.P.J.A.; Visualization, C.B.T. and C.V.M. All authors have read and agreed to the published version of the manuscript.

Funding: This work was supported by the Department of Science and Technology—Philippine Council for Industry, Energy and Emerging Technology Research and Development (DOST-PCIEERD) Project No. 04609.

Data Availability Statement: Data are contained within the article.

Acknowledgments: The authors are grateful to the Central Mindanao University administration for the assistance during the duration of this research. Special acknowledgment is also due to the Department of Civil Engineering for the moral support in the conduct of the study. Moreover, the authors acknowledge the assistance of John Paul Manlulu and Jet Ryan Delfinado during the collection and preparation of materials for the experiments.

Conflicts of Interest: The authors declare no conflict of interest.

References

1. Appleton, J.D.; Williams, U.T.M.; Breward, N.; Apostol, A.; Miguel, J.; Miranda, C. Mercury contamination associated with artisanal gold mining on the island of Mindanao, the Philippines. *Sci. Total Environ.* **1999**, *228*, 95–109. [[CrossRef](#)] [[PubMed](#)]
2. Tabelin, C.B.; Silwamba, M.; Paglinawan, F.C.; Mondejar, A.J.S.; Duc, H.G.; Resabal, V.J.; Opiso, E.M.; Igarashi, T.; Tomiyama, S.; Ito, M.; et al. Solid-phase partitioning and release-retention mechanisms of copper, lead, zinc and arsenic in soils impacted by artisanal and small-scale gold mining (ASGM) activities. *Chemosphere* **2020**, *260*, 127574. [[CrossRef](#)]
3. Aseniero, J.P.; Opiso, E.M.; Banda, M.H.B.; Tabelin, C.B. Potential Utilization of artisanal gold-mine tailings as geopolymeric source material: A preliminary investigation. *SN Appl. Sci.* **2019**, *1*, 35. [[CrossRef](#)]
4. Opiso, E.M.; Aseniero, J.P.; Banda, M.H.T.; Tabelin, C.B. Solid-phase partitioning of mercury in artisanal gold mine tailings from selected key areas in Mindanao, Philippines, and its implications for mercury detoxification. *Waste Manag. Res.* **2018**, *36*, 269–276. [[CrossRef](#)]
5. Opiso, E.M.; Tabelin, C.; Maestre, C.V.; Aseniero, J.P.; Park, I.; Villacorte-Tabelin, M. Synthesis and Characterization of Coal Fly Ash and Palm Oil Fuel Ash modified Artisanal and Small-scale Gold Mine (ASGM) tailings based geopolymer using sugar mill lime sludge as Ca-based activator. *Heliyon* **2021**, *7*, e06654. [[CrossRef](#)]
6. Ahmari, S.; Zhang, L. Durability and leaching behavior of mine tailings-based geopolymer bricks. *Constr. Build. Mater.* **2013**, *44*, 743–750. [[CrossRef](#)]
7. Zeng, J.; Tabelin, C.B.; Gao, W.; Tang, L.; Luo, X.; Ke, W.; Jiang, J.; Xue, S. Heterogeneous distributions of heavy metals in the soil-groundwater system empowers the knowledge of the pollution migration at a smelting site. *Chem. Eng. J.* **2022**, *454*, 140307. [[CrossRef](#)]
8. Tabelin, C.B.; Uyama, A.; Tomiyama, S.; Villacorte-Tabelin, M.; Phengsaart, T.; Silwamba, M.; Jeon, S.; Park, I.; Arima, T.; Igarashi, T. Geochemical audit of a historical tailings storage facility in Japan: Acid mine drainage formation, zinc migration and mitigation strategies. *J. Hazard. Mater.* **2022**, *438*, 129453. [[CrossRef](#)]
9. Jeon, S.; Tabelin, C.B.; Park, I.; Nagata, Y.; Ito, M.; Hiroyoshi, N. Ammonium thiosulfate extraction of gold from printed circuit boards (PCBs) of end-of-life mobile phones and its recovery from pregnant leach solution by cementation. *Hydrometallurgy* **2020**, *191*, 105214. [[CrossRef](#)]
10. Argane, R.; Benzaazoua, M.; Hakkou, R.; Bouamrane, A. Reuse of base-metal tailings as aggregates for rendering mortars: Assessment of immobilization performances and environmental behavior. *Constr. Build. Mater.* **2015**, *96*, 296–306. [[CrossRef](#)]
11. Moukannaa, S.; Loutou, M.; Benzaazoua, M.; Vitola, L.; Alami, J.; Hakkou, R. Recycling of phosphate mine tailings for the production of geopolymers. *J. Clean. Prod.* **2018**, *185*, 891–903. [[CrossRef](#)]
12. Mabroum, S.; Aboulayt, A.; Taha, Y.; Benzaazoua, M.; Semlal, N.; Hakkou, R. Elaboration of geopolymers based on clays by-products from phosphate mines for construction applications. *J. Clean. Prod.* **2020**, *261*, 121317. [[CrossRef](#)]
13. Mabroum, S.; Taha, Y.; Benzaazoua, M.; Hakkou, R. Recycling of marls from phosphate by-products to produce alkali-activated geopolymers. *Mater. Today Proc.* **2022**, *51*, 1931–1936. [[CrossRef](#)]
14. Alelvan, G.M.; Ferreira, J.W.d.S.; Casagrande, M.D.T.; Consoli, N.C. Proposal of New Construction Material: Polymer-Stabilized Gold Ore Tailings Composite. *Sustainability* **2022**, *14*, 13648. [[CrossRef](#)]

15. Rybak, J.; Gorbatyuk, S.M.; Kongar-Syuryun, C.B.; Khairutdinov, A.M.; Tyulyaeva, Y.S.; Makarov, P.S. Utilization of mineral waste: A method for expanding the mineral resource base of a mining and smelting company. *Metallurgist* **2021**, *64*, 851–861. [[CrossRef](#)]
16. Hefni, M.; Ahmed, H.A.M.; Omar, E.S.; Ali, M.A. The potential re-use of Saudi mine tailings in mine backfill: A path towards sustainable mining in Saudi Arabia. *Sustainability* **2021**, *13*, 6204. [[CrossRef](#)]
17. Rybak, J.; Adigamov, A.; Kongar-Syuryun, C.; Khayrutdinov, M.; Tyulyaeva, Y. Renewable-Resource Technologies in Mining and Metallurgical Enterprises Providing Environmental Safety. *Minerals* **2021**, *11*, 1145. [[CrossRef](#)]
18. Šajn, R.; Ristović, I.; Čeplak, B. Mining and Metallurgical Waste as Potential Secondary Sources of Metals—A Case Study for the West Balkan Region. *Minerals* **2022**, *12*, 547. [[CrossRef](#)]
19. Zglinicki, K.; Szamałek, K.; Wołkowicz, S. Critical Minerals from Post-Processing Tailing. A Case Study from Bangka Island, Indonesia. *Minerals* **2021**, *11*, 352. [[CrossRef](#)]
20. Wang, Q.; Li, J.; Wang, F.; Sakanakura, H.; Tabelin, C.B. Effective immobilization of geogenic As and Pb in excavated marine sedimentary material by magnesite under wet–dry cycle, freeze–thaw cycle, and anaerobic exposure scenarios. *Sci. Total Environ.* **2022**, *848*, 157734. [[CrossRef](#)]
21. Silwamba, M.; Ito, M.; Hiroyoshi, N.; Tabelin, C.B.; Hashizume, R.; Fukushima, T.; Park, I.; Jeon, S.; Igarashi, T.; Sato, T.; et al. Recovery of Lead and Zinc from Zinc Plant Leach Residues by Concurrent Dissolution-Cementation Using Zero-Valent Aluminum in Chloride Medium. *Metals* **2020**, *10*, 531. [[CrossRef](#)]
22. McDonald, J.E.D.; Roache, S.C.; Kawatra, S.K. Repurposing mine tailings: Cold bonding of siliceous iron ore tailings. *Miner. Metall. Process.* **2016**, *33*, 47–52. [[CrossRef](#)]
23. Perdeli Demirkan, C.; Smith, N.M.; Duzgun, S. A Quantitative Sustainability Assessment for Mine Closure and Repurposing Alternatives in Colorado, USA. *Resources* **2022**, *11*, 66. [[CrossRef](#)]
24. Han, L.J.; Li, J.S.; Xue, Q.; Guo, M.Z.; Wang, P.; Poon, C.S. Enzymatically induced phosphate precipitation (EIPP) for stabilization/solidification (S/S) treatment of heavy metal tailings. *Constr. Build. Mater.* **2022**, *314*, 125577. [[CrossRef](#)]
25. Qaidi, S.M.; Atrushi, D.S.; Mohammed, A.S.; Ahmed, H.U.; Faraj, R.H.; Emad, W.; Tayeh, B.A.; Najm, H.M. Ultra-high-performance geopolymer concrete: A review. *Constr. Build. Mater.* **2022**, *346*, 128495. [[CrossRef](#)]
26. Mabroum, S.; Moukannaa, S.; El Machi, A.; Taha, Y.; Benzaazoua, M.; Hakkou, R. Mine wastes based geopolymers: A critical review. *Clean. Eng. Technol.* **2020**, *1*, 100014. [[CrossRef](#)]
27. Ouffa, N.; Benzaazoua, M.; Belem, T.; Trauchessec, R.; Lecomte, A. Alkaline dissolution potential of aluminosilicate minerals for the geosynthesis of mine paste backfill. *Mater. Today Commun.* **2020**, *24*, 101221. [[CrossRef](#)]
28. Abdel-Gawwad; Abo-El-Enein. A novel method to produce dry geopolymer cement powder. *HBRC J.* **2016**, *12*, 13–24. [[CrossRef](#)]
29. Abdul Rahim, R.H.; Rahmiati, T.; Azizli, K.A.; Man, Z.; Nuruddin, M.F.; Ismail, L. Comparison of using NaOH and KOH Activated Fly ash -based geopolymer on mechanical properties. *Mater. Sci. Forum* **2015**, *803*, 179–184. [[CrossRef](#)]
30. Kiventera, J.; Golek, L.; Yliniemi, J.; Ferreira, V.; Deja, J.; Illikainen, M. Utilization of sulphidic tailings from gold mine as raw materials in geopolymerization. *Int. J. Miner. Process.* **2016**, *149*, 104–110. [[CrossRef](#)]
31. Ouffa, N.; Trauchessec, R.; Benzaazoua, M.; Lecomte, A.; Belem, T. A methodological approach applied to elaborate alkali-activated binders for mine paste backfills. *Cem. Concr. Compos.* **2022**, *127*, 104381. [[CrossRef](#)]
32. Hertel, T.; Blanpain, B.; Pontikes, Y. A proposal for a 100% use of bauxite residue towards inorganic polymer mortar. *J. Sustain. Metall.* **2016**, *2*, 394–404. [[CrossRef](#)]
33. Ahmari, S.; Zhang, L. Production of eco-friendly bricks from copper mine tailings through geopolymerization. *Construct. Build. Mater.* **2012**, *29*, 323–331. [[CrossRef](#)]
34. Kuranchie, F.A.; Shukla, S.K.; Habibi, D. Utilisation of iron ore mine tailings for the production of geopolymer bricks. *Int. J. Min. Reclam. Environ.* **2016**, *30*, 92–114. [[CrossRef](#)]
35. Pacheco-Torgal, F.; Castro-Gomes, J.; Jalali, S. Investigations about the effect of aggregates on strength and microstructure of geopolymeric mine waste mud binders. *Cem. Concr. Res.* **2007**, *37*, 933–941. [[CrossRef](#)]
36. Jiao, X.; Zhang, Y.; Chen, T. Thermal stability of a silica-rich vanadium tailing based geopolymer. *Construct. Build. Mater.* **2013**, *38*, 43–47. [[CrossRef](#)]
37. Singh, B.; Ishwarya, G.; Gupta, M.; Bhattacharyya, S.K. Geopolymer concrete: A review of some recent developments. *Constr. Build. Mater.* **2015**, *85*, 78–90. [[CrossRef](#)]
38. Khankhaje, E.; Hussin, M.W.; Mirza, J.; Rafieizonooz, M.; Salim, M.R.; Siong, H.C.; Warid, M.N.M. On blended cement and geopolymer concretes containing palm oil fuel ash. *Mater. Des.* **2016**, *89*, 385–398. [[CrossRef](#)]
39. Islam, A.; Alengaram, U.J.; Jumaat, M.Z.; Bashar, I.I.; Kabir, S.A. Engineering properties and carbon footprint of ground granulated blast-furnace slag-palm oil fuel ash-based structural geopolymer concrete. *Constr. Build. Mater.* **2015**, *101*, 503–521. [[CrossRef](#)]
40. Huseien, G.F.; Mirza, J.; Ismail, M.; Hussin, M.W. Influence of different curing temperatures and alkali activators on properties of GBFS geopolymer mortars containing fly ash and palm-oil fuel ash. *Constr. Build. Mater.* **2016**, *125*, 1229–1240. [[CrossRef](#)]
41. Gitari, M.W.; Akinyemi, S.A.; Thobakgale, R. Physicochemical and mineralogical characterization of musina mine copper and new onion gold mine tailings: Implications for fabrication of beneficial geopolymeric construction of materials. *J. Afr. Earth Sci.* **2017**, *137*, 218–228. [[CrossRef](#)]
42. Ranjbar, N.; Mehrali, M.; Behnia, A.; Alengaram, U.J.; Jumaat, M.Z. Compressive strength and microstructural analysis of fly ash/palm oil fuel ash based geopolymer mortar. *Mater. Des.* **2014**, *59*, 532–539. [[CrossRef](#)]

43. Bashar, I.I.; Alengaram, U.J.; Jumaat, M.Z.; Islam, A.; Santhi, H.; Sharmin, A. Engineering properties and fracture behaviour of high volume palm oil fuel ash based fibre reinforced geopolymer concrete. *Constr. Build. Mater.* **2016**, *111*, 286–297. [[CrossRef](#)]
44. Asamoah, R.K.; Zanin, M.; Gascooke, J.; Skinner, W.; Addai-Mensah, J. Refractory gold ores and concentrates part 1: Mineralogical and physico-chemical characteristics. *Miner. Process Extr. Metall.* **2021**, *130*, 240–252. [[CrossRef](#)]
45. Park, I.; Tabelin, C.B.; Seno, K.; Jeon, S.; Inano, H.; Ito, M.; Hiroyoshi, N. Carrier-microencapsulation of arsenopyrite using Al-catecholate complex: Nature of oxidation products, effects on anodic and cathodic reactions, and coating stability under simulated weathering conditions. *Heliyon* **2020**, *6*, e03189. [[CrossRef](#)]
46. Chen, Y.; Furmann, A.; Mastalerz, M.; Schimmelmann, A. Quantitative analysis of shales by KBr-FTIR and micro-FTIR. *Fuel* **2014**, *116*, 538–549. [[CrossRef](#)]
47. Aines, R.D.; Rossman, G.R. Water in minerals? A peak in the infrared. *J. Geophys. Res.* **1984**, *89*, 4059–4071. [[CrossRef](#)]
48. Chernyshova, I.V. An in situ FTIR study of galena and pyrite oxidation in aqueous solution. *J. Electroanal. Chem.* **2003**, *558*, 83–98. [[CrossRef](#)]
49. Andersen, F.A.; Brecevic, L. Infrared spectra of amorphous and crystalline calcium carbonate. *Acta Chem. Scand.* **1991**, *45*, 1018–1024. [[CrossRef](#)]
50. Yuniati, M.; Hijarima, T.; Miki, H.; Sasaki, K. Silicate covering layer on pyrite surface in the presence of silicon-catechol complex for acid mine drainage prevention. *Mater. Trans.* **2015**, *56*, 1733–1741. [[CrossRef](#)]
51. Carlson, L.; Bigham, J.M.; Schwertmann, U.; Kyek, A.; Wagner, F. Scavenging of As from acid mine drainage by schwertmannite and ferrihydrite: A comparison with synthetic analogues. *Environ. Sci. Technol.* **2002**, *36*, 1712–1719. [[CrossRef](#)] [[PubMed](#)]
52. Liu, L.P.; Cui, X.M.; He, Y.; Liu, S.D.; Gong, S.Y. The phase evolution of phosphoric acid-based geopolymers at elevated temperatures. *J. Mater. Lett.* **2012**, *66*, 10–12. [[CrossRef](#)]
53. Selami, M.; Barre, M.; Toumi, M. Synthesis, thermal properties of and electrical conductivity of phosphoric acid-based geopolymer with metakaolin. *Appl. Clay Sci.* **2019**, *180*, 105192. [[CrossRef](#)]
54. Meeussen, J.C.L.; Van Riemsdijk, W.H.; Van der Zee, S.E.A.T.M. Transport of complexed cyanide in soil. *Geoderma* **1995**, *67*, 73–85. [[CrossRef](#)]
55. Nikolov, A.; Rostovsky, I.; Nugteren, H. Geopolymer materials based on natural zeolite. *Case Stud. Construct. Mater.* **2017**, *6*, 198–205. [[CrossRef](#)]
56. Khalifa, A.Z.; Cizer, Ö.; Pontikes, Y.; Heath, A.; Patureau, P.; Bernal, S.A.; Marsh, A.T. Advances in alkali-activation of clay minerals. *Cem. Concr. Res.* **2022**, *132*, 106050. [[CrossRef](#)]
57. Marsh, A.; Heath, A.; Patureau, P.; Evernden, M.; Walker, P. Phase formation behaviour in alkali activation of clay mixtures. *Appl. Clay Sci.* **2019**, *175*, 10–21. [[CrossRef](#)]
58. du Plessis, C.A.; Lambert, H.; Gärtner, R.S.; Ingram, K.; Slabbert, W.; Eksteen, J.J. Lime use in gold processing—A review. *Miner. Eng.* **2021**, *174*, 107231. [[CrossRef](#)]
59. Abraitis, P.K.; Patrick, R.A.D.; Vaughan, D.J. Variations in the compositional, textural and electrical properties of natural pyrite: A review. *Int. J. Miner. Process.* **2004**, *74*, 41–59. [[CrossRef](#)]
60. He, P.; Wang, M.; Fu, S.; Jia, D.; Yan, S.; Yuan, J.; Xu, J. Effects of Si/Al ratio on the structure and properties of metakaolin based geopolymer. *Ceram. Int.* **2016**, *42*, 14416–14422. [[CrossRef](#)]
61. Luna-Galiano, Y.; Fernández-Pereira, C.; Izquierdo, M. Contributions to the study of porosity in fly ash-based geopolymers. Relationship between degree of reaction, porosity and compressive strength. *Mater. De Construcción* **2016**, *66*, e098. [[CrossRef](#)]
62. Caldeira, C.L.; Ciminelli, V.S.; Osseo-Asare, K. The role of carbonate ions in pyrite oxidation in aqueous systems. *Geochim. Cosmochim. Acta* **2010**, *74*, 1777–1789. [[CrossRef](#)]
63. Nicholson, R.V.; Gillham, R.W.; Reardon, E.J. Pyrite oxidation in carbonate-buffered solution: 1. Experimental kinetics. *Geochim. Cosmochim. Acta.* **1988**, *52*, 1077–1085. [[CrossRef](#)]

Disclaimer/Publisher’s Note: The statements, opinions and data contained in all publications are solely those of the individual author(s) and contributor(s) and not of MDPI and/or the editor(s). MDPI and/or the editor(s) disclaim responsibility for any injury to people or property resulting from any ideas, methods, instructions or products referred to in the content.